# Scaffolding of Enzymes on Virus Nanoarrays: Effects of Confinement and Virus Organization on Biocatalysis

*Anisha N. Patel, Agnès Anne,* Arnaud Chovin, Christophe Demaille,* Eric Grelet, Thierry Michon,* and Cécilia Taofifenua*

***O**rganizing active enzyme molecules on nanometer-sized scaffolds is a promising strategy for designing highly efficient supported catalytic systems for biosynthetic and sensing applications. This is achieved by designing model nanoscale enzymatic platforms followed by thorough analysis of the catalytic activity. Herein, the virus fd bacteriophage is considered as an enzyme nanocarrier to study the scaffolding effects on enzymatic activity. Nanoarrays of randomly oriented, or directionally patterned, fd bacteriophage virus are functionalized with the enzyme glucose oxidase (GOx), using an immunological assembly strategy, directly on a gold electrode support. The scaffolding process on the virus capsid is monitored in situ by AFM (atomic force microscopy) imaging, while cyclic voltammetry is used to interrogate the catalytic activity of the resulting functional GOx-fd nanoarrays. Kinetic analysis reveals the ability to modulate the activity of GOx via nanocarrier patterning. The results evidence, for the first time, enhancement of the enzymatic activity due to scaffolding on a filamentous viral particle.*

Dr. A. N. Patel, Dr. A. Anne, Dr. A. Chovin,
Dr. C. Demaille, Dr. C. Taofifenua
Laboratoire d'Electrochimie Moléculaire
UMR 7591 CNRS
Université Paris Diderot
Sorbonne Paris Cité
15 rue Jean-Antoine de Baïf
F-75205 Paris Cedex 13, France
E-mail: anne@univ-paris-diderot.fr;
demaille@univ-paris-diderot.fr
Dr. E. Grelet
Centre de Recherche Paul-Pascal
UPR 8641 CNRS
Université de Bordeaux
115 avenue Schweitzer, 33600 Pessac, France
Dr. T. Michon
Biologie du Fruit et Pathologie
UMR 1332 INRA
Université de Bordeaux
71 avenue Edouard Bourlaux, CS20032
33882 Villenave d'Ornon Cedex, France
E-mail: tmichon@bordeaux.inra.fr

DOI: 10.1002/smll.201603163

## 1. Introduction

In living cells, many enzymes involved in metabolic pathways are organized in ordered supramolecular enzyme complexes, supported by scaffold proteins.[1] This nanoscale organization endows biological synthetic pathways with unmatched efficiency and specificity. It is therefore highly tempting to try mimicking this natural enzyme organization for designing bioreactors enabling the synthesis of valuable metabolites of industrial or medical importance, but also for enhancing the sensitivity of enzyme-based sensors.[2] In parallel, fundamental studies are also required to try to understand how spatial organization modulates the catalytic efficiency of natural scaffolded enzymatic systems. To achieve this goal, model nanoscale enzymatic platforms have been designed and their functional behavior interrogated.[2] In these systems enzymes are typically assembled at the surface of, or within, nanometer-sized scaffolds, referred to as enzyme nanocarriers,[3] which may be inorganic nanoparticles, liposomes, polymersomes, DNA origamis, or even viruses.[4] Of particular interest is the co-immobilization of

  

several different enzymes on a single nanocarrier in order to reconstitute enzymatic cascades. In this arrangement multiple enzymes catalyze a series of conversions. This sequential organization is supposed to be a key factor for the efficiency of natural enzymatic nanosystems.[5] Several artificial enzymatic cascades have been recently assembled on various supports and catalytic enhancement has indeed been observed in some cases.[6] Yet it has, surprisingly, also been shown that even much simpler scaffolded enzymatic systems, involving only a single type of enzyme (and not a cascade), can equally display enhanced catalysis.[7] This effect has been reported for many different types of enzymes immobilized on various nanometer-sized particles, ranging from gold nanoparticles to carbon nanotubes and graphene nanosheets.[8] Virus particles have also attracted a lot of attention as enzyme nanocarriers to study scaffolding effects on enzymatic activity.[9] The reasons for such an interest are that viruses are nanometer to micrometer-sized monodisperse particles, offering a large shape diversity and a highly ordered architecture specifically enabling spatially controlled assembly of biomolecules. Besides, viral particles themselves can be patterned onto solid supports using top-down technologies,[10] which opens the yet unexplored possibility of producing highly ordered arrays of functional viral particles with order-related properties. In literature, one can find several reports where the catalytic activity of various types of such virus-supported enzymatic systems has been assessed, the enzyme molecules being either attached to the surface of the virus[9c,f,j,k] or encapsulated inside.[9b,d,e,g–j] However, in spite of these studies, the effects on the enzymatic performance of enzymes attached to viral particles remains unclear as they differ depending on the system considered.[9a] In many cases, enzymes borne by virus particles were simply found to display the same activity as when freely dispersed in solution.[9b,c,f,h–k] In other instances, the activity of virus-bound enzymes was found to be either enhanced[9e] or inhibited.[9d,g] Interpretation of these variations is quite complex since many factors, such as substrate mass transport to/within the enzyme nanocarrier, or macromolecular crowding, can simultaneously modulate the overall reaction rate. The question of whether classical Michaelis–Menten kinetics can be applied to analyze the behavior of virus-scaffolded enzymatic systems has even been raised.[9a]

In order to address these issues, herein, we assemble randomly oriented, or directionally patterned, arrays of fd bacteriophage, as the viral scaffold, onto a gold electrode surface. The surface-immobilized bacteriophage particles are immunodecorated by the enzyme glucose oxidase (GOx) by making use of virus-specific antibodies, further recognized by GOx-conjugated antibodies. The step-by-step immunological construction of the enzymatic assembly on the virus protein shell (capsid) is monitored in situ by atomic force microscopy (AFM) imaging. The catalytic activity of the final electrode-supported functional virus-nanoarrays is probed by cyclic voltammetry using the one-electron mediator ferrocenedimethanol as the GOx cosubstrate. This configuration allows the kinetic behavior of the virus-supported enzyme to be fully characterized.

The individual values of the enzymatic rate constants are determined for both directionally patterned and randomly oriented glucose oxidase-functionalized viruses, and compared to the values measured for the enzyme immunologically assembled as a monolayer onto gold electrodes in order to reveal enzyme scaffolding and scaffold-ordering kinetic effects.

## 2. Results and Discussion

Fd bacteriophage was chosen as the enzyme nanocarrier as it is closely related to the M13 bacteriophage commonly used for nanobiotechnological[11] and sensing applications.[12] The fd bacteriophage is a ≈880 nm long, 6.6 nm diameter semi-rigid filamentous virus specifically infecting *Escherichia coli* bacteria (see **Figure 1**).[13] It is composed of ≈2700 copies of a major coat protein (P8), packed around a single-stranded circular DNA, and of a few copies of four other proteins constituting each of its (dissimilar) extremities. The isoelectric pH of fd is ≈4.2, hence in physiological conditions the phage capsid is highly negatively charged, displaying a linear charge density of ≈10 $e^-$ $nm^{-1}$ at pH 7.4.[13]

GOx was employed as the enzyme to build a functional nanoscaffolded catalytic system due to its importance and broad use in biosensing. Moreover, its kinetics, both in solution and on surfaces, are very well established,[14] and as a redox enzyme, its catalytic behavior can be very finely probed by electrochemical techniques.[15] An antigen-antibody reaction was used for functionalization of fd nanocarriers with enzymes as this method has previously proven to allow for the immobilization of GOx onto surfaces whilst fully preserving its catalytic activity,[16] allowing for the kinetic effects of nanoscaffolding to be studied.

### 2.1. Step-by-Step Assembly of Random Arrays of GOx Immunodecorated fd

An original aspect of the present work is that the virus-borne enzymatic system is directly assembled on a sensing surface, a gold electrode, rather than assembling it in solution as commonly done. The major advantage of direct surface assembly is that separation of the building elements (free antibodies) and decorated virus particles is immediate. However, strong binding of fd to the electrode surface is required.

Spontaneous adsorption of fd as a way of anchoring the virus to an ultraflat template-stripping (TS) gold surface was first attempted, however, in contrast to what has been observed with other viruses (lettuce mosaic virus and potato virus A),[17] mere adsorption from solution does not result in stable enough anchoring of fd to bare gold. Hence, we modified the gold surface with a positively charged self-assembled layer of cysteamine, promoting electrostatic adhesion of the negatively charged fd particles (at pH 7.4).[18] Once fd was adsorbed on a cysteaminated surface, the surface was then imaged in situ (PB (phosphate buffer), pH 7.4) with AFM tapping. For example, 5 μm × 5 μm topographical image (Figure 1A) showed numerous filamentous ≈900 nm long and ≈6 nm high particles, ascribable to intact individual fd virions randomly organized on the surface. The viruses seen in the

  

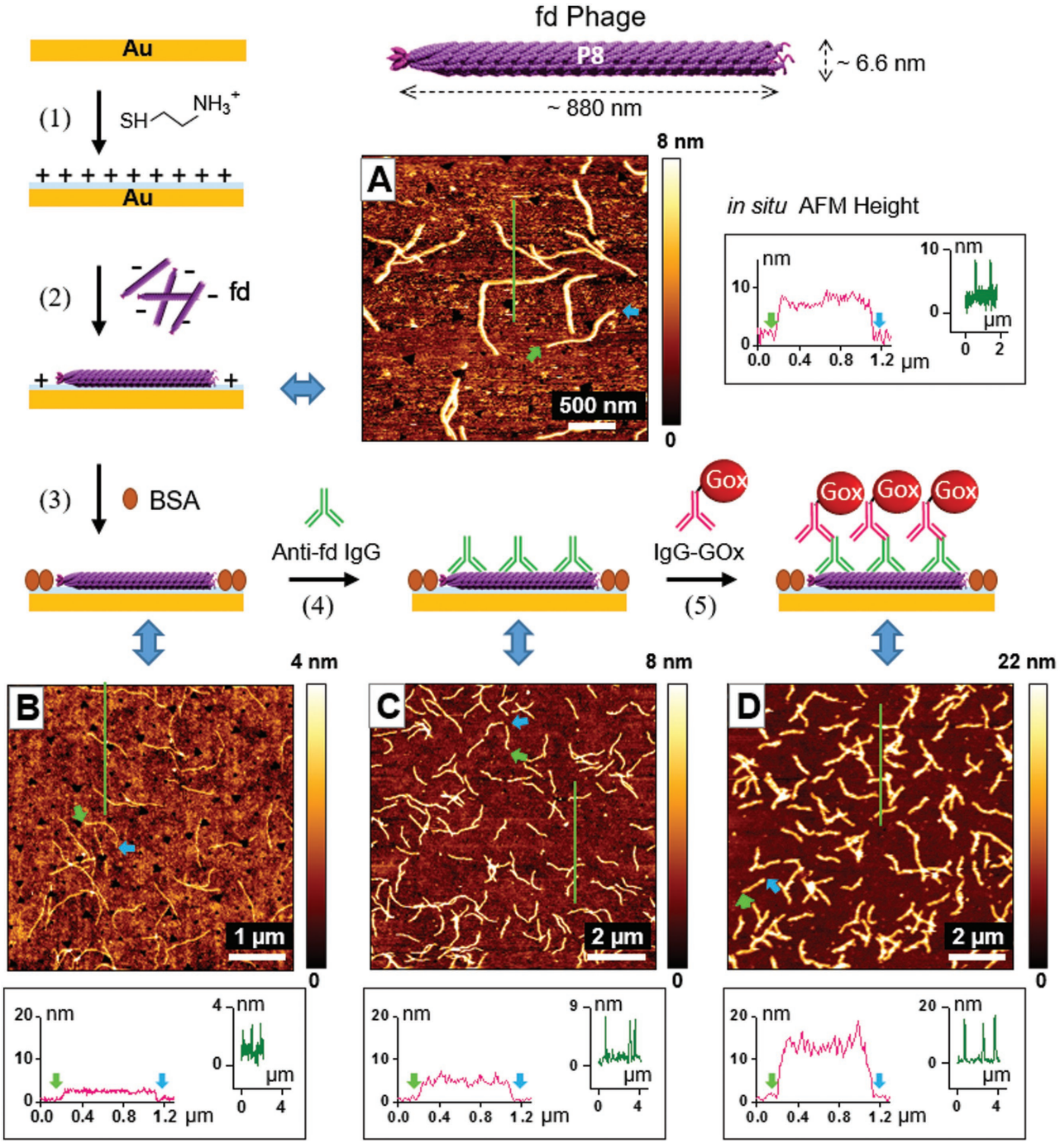


**Figure 1.** Schematic representation of fd phage and the sequential steps for construction of GOx-decorated fd random nanoarrays on TS-gold. In situ tapping mode AFM images of the arrays at each assembly acquired immediately following: A) Adsorption of fd, B) surface backfilling by BSA, C) recognition of fd by the primary anti-fd IgG, and D) recognition of the primary IgG by the GOx-conjugated secondary antibody. Below each image are cross-sections taken: (i) along the individual fd particles marked by arrows (pink traces) and (ii) along the vertical green lines shown in the image (green traces). fd concentration used for adsorption $[fd]_{ads} = 1.9$ µg mL$^{-1}$. $\gamma_{fd} \approx 1.7$ particles µm$^{-2}$.

images appear much wider than they actually are (apparent width ≈80 nm) due to a well-known tip convolution artifact. Hence, the apparent widths of viruses are only considered qualitatively.

A 1 h bovine serum albumin (BSA) backfilling step was carried out to prevent nonspecific adsorption of the biomolecules involved in the construction processes. The presence of the BSA layer was revealed in AFM images by an increased roughness in the background-areas extending between the virus particles (Figure 1B). An apparent 4 nm decrease in height of the virus particles was also observed, indicative of partial embedding of the fd particles by the surrounding BSA molecules.[15] Subsequently, the surface was exposed to the primary anti-fd antibody for 45 min. Post in situ AFM imaging showed a remarkable increase in virus height and width indicative of effective immunobinding of the anti-fd

  

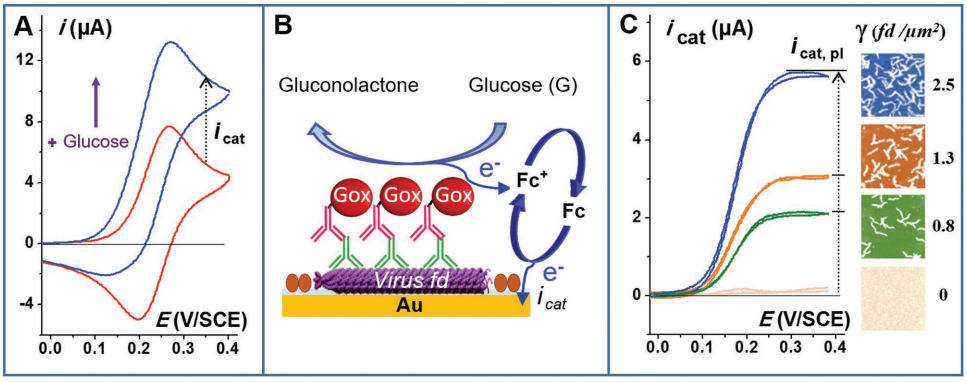


**Figure 2.** A) CV, *i* versus *E*, of ferrocenedimethanol (Fc) ($0.25 \times 10^{-3}$ M in deoxygenated $10 \times 10^{-3}$ M PB, pH 7.4) recorded at a gold electrode bearing GOx-decorated fd particles, either in the absence (red trace) or in the presence (blue trace) of $100 \times 10^{-3}$ M glucose. B) Schematic representation of the catalytic cycle taking place at the GOx-immunodecorated fd particles adsorbed on the surface. C) Purely catalytic CVs, $i_{cat}$ versus *E*, derived for surfaces bearing either no viruses (bottom, pink beige trace) or GOx-decorated fd particles of coverages $\gamma_{fd}$: 0.5, 1.3, and 2.5 particles $\mu m^{-2}$ (green, orange, and blue traces, respectively). In situ AFM images of the surfaces corresponding to each catalytic CV are also shown. Scan rate 10 mV $s^{-1}$. $T = 25$ °C.

immunoglobulin G (IgG) to the virus surface (Figure 1C). The increase in virus height was of ≈6–8 nm, which corresponds to the dimension of an IgG molecule (≈10 nm)—albeit slightly smaller.[19] It is widely known that during tapping mode AFM imaging of soft materials, including biomolecules, small height discrepancies are observed owing to sample–tip interaction. Moreover, it was previously reported that IgGs bound to virus capsids are imperfectly sensed by AFM probes,[20] likely due to their inherent flexibility. Both effects likely contribute to these observations herein.

Finally, the surface was exposed to the glucose oxidase-conjugated antirabbit antibody (IgG-GOx) for ≈15 h (overnight). Subsequent AFM images showed that the apparent width and height of the virus particles had further increased (see Figure 1D). The 10–15 nm increase in height was close to the estimated molecular size of the IgG-GOx conjugate (≈20 nm) and thus demonstrates the effective immunoassembly of the conjugate onto the fd particles. Note, the change in virus height and width was observed for all of the viruses in the images and along the full length of each of them, suggesting a very high degree of immunodecoration by the IgG-GOx conjugate. Importantly, besides virus particles, very few objects can be seen on the surface that are likely sparsely adsorbed immunocomplexes, confirming specific immunodecoration of fd viruses with enzyme tagged antibodies is achieved. The randomly oriented nanoarrays appear partly intertwined but are easy to individualize and count, allowing for an average virus coverage on the surface ($\gamma_{fd}$) to be obtained. Varying the fd solution concentration enabled the $\gamma_{fd}$ to be tuned from 0.5 up to 2 particles $\mu m^{-2}$ (Figure S1, Supporting Information).

### 2.2. Probing the Catalytic Activity of Randomly Oriented GOx-fd Nanoarrays

Voltammetric measurements were carried out to probe the catalytic activity of random GOx-fd nanoarrays in deoxygenated PB pH 7.4 containing ferrocenedimethanol, Fc. A representative cyclic voltammogram (CV) is shown in **Figure 2**A (red trace). The voltammogram is typical of diffusive redox species undergoing fast and reversible (i.e., Nernstian) (one) electron transfer at the electrode surface; the peak current of the forward wave is proportional to the square root of the scan rate and the peak-to-peak separation is close to 60 mV. The average of the forward and return peak potentials is ≈0.235 V per saturated calomel electrode (SCE), corresponding to the standard potential $E°$ of ferrocenedimethanol as measured at a bare gold electrode.[21] The data confirm electron transfer between the underlying gold electrode and freely diffusing Fc is not inhibited by the (bio)molecular species present on the electrode surface. Importantly, in situ AFM imaging carried after CV measurements shows the GOx-fd arrays intact, verifying the virus nanoarrays are not damaged during electrochemical interrogation (see Supporting Information).

Upon injection of glucose into the Fc solution, to a final concentration of $100 \times 10^{-3}$ M, the CV signal markedly increased in intensity, whilst seemingly losing its reversibility (see Figure 2A, blue trace), an expected response evidencing enzymatic catalysis of glucose oxidation, where GOx uses the oxidized form of Fc (the ferroceniumdimethanol, $Fc^+$) produced at the electrode as a redox cosubstrate.[16] The resulting regeneration of Fc triggers the catalytic cycle represented in Figure 2B.

The GOx-catalyzed oxidation of glucose mediated by ferrocene species can be represented by the following sequence of reactions:[15]

$$\mathrm{P} \overset{E^\circ}{\leftrightarrows} \mathrm{Q}^+ + \mathrm{e}^-$$

$$2\mathrm{Q} + \mathrm{EFADH_2} \xrightarrow{k_{ox}} 2\mathrm{P} + \mathrm{EFAD} + 2\mathrm{H}^+$$

$$\mathrm{G} + \mathrm{EFAD} \underset{k_{-1}}{\overset{k_1}{\leftrightarrow}} \mathrm{EFAD-G}$$

$$\mathrm{EFAD-G} \xrightarrow{k_{cat}} \mathrm{EFADH_2} + \mathrm{GI}$$

where P and Q are the reduced (Fc) or oxidized ($Fc^+$) forms of the ferrocene cosubstrate. $EFADH_2$, EFAD, and EFAD-G represent the prosthetic group of GOx (the enzyme-bound flavin adenine dinucleotide, EFAD) in its reduced state, in its oxidized state, and its complexed state, respectively. G is glucose and Gl is the enzymatic product gluconolactone.

Full kinetic characterization of enzyme activity can be carried out by analysis of CVs using a methodology introduced previously in a related context.[16] In this earlier work, GOx was immunologically immobilized onto electrodes bearing a layer of adsorbed IgGs. It was shown that the immunological immobilization permitted a positioning of the enzyme sufficiently far away from the electrode surface to not be denaturated, but sufficiently close enough for diffusional limitation of the $Fc^+$ cosubstrate to be negligible. Hence, the entire flux of Fc produced by the enzyme molecules is then collected at the electrode.

The above conditions are also fulfilled here as the immobilization strategy is the same and the enzyme-electrode separation is equally small (see "estimation of $Fc^+$ diffusion layer" in the Supporting Information). As demonstrated previously, in such a case, the following statements apply

(i) The CV current, $i$, recorded during enzymatic catalysis is simply given by

$$i = i_0 + i_{cat} \tag{1}$$

where $i_0$ is the current recorded in the absence of catalysis (i.e., without glucose), and $i_{cat}$ is the current specifically due to the catalytic activity of the enzyme. The catalytic current, $i_{cat}$, is directly related to the rate of the enzymatic reaction $v_{ez}$, and, assuming Michaelis–Menten kinetics, is given by

$$i_{cat} = 2FSv_{ez} = \frac{2Fn_E k_{cat}}{1 + \frac{K_M^{Fc}}{Q_0} + \frac{K_M^G}{[G]}} \tag{2}$$

where $K_M^{Fc} = k_{cat}/k_{ox}$ is the ratio of the enzyme turnover upon the kinetic constant for enzyme oxidation by ferrocenium $Fc^+$ and $K_M^G = (k_{cat} + k_{-1})/k_1$ is the Michaelis constants for glucose. [G] is the glucose concentration sensed by the enzyme, $n_E$ is the number of moles of enzyme species on the surface, as defined in the above kinetic scheme. Hence, $n_E$ is actually the total amount of enzyme-bound flavin.

(ii) The $Fc^+$ concentration "as seen" by the surface-confined enzyme equals $Q_0$, the $Fc^+$ concentration at the electrode surface, which is simply related to the electrode potential, $E$, by

$$\text{Nernst law}: Q_0 = C_P^\circ/(1 + \exp(-F(E - E^\circ)/RT)) \tag{3}$$

where $C_P^\circ$ is the bulk concentration of cosubstrate and $E°$ is the standard potential of the $Fc/Fc^+$ redox couple.

As suggested by Equation (1), $i_{cat}$ is experimentally determined by subtracting the CV signal recorded in the absence of catalysis (of glucose) from the signal recorded after injection of glucose (see Figure 2A). Figure 2C (blue trace) shows the result of this subtraction, a sigmoidal-shaped $i_{cat}$ versus $E$ steady state voltammogram typical of a purely catalytic regime, as predicted by Equations (2) and (3), containing all the kinetic information characterizing the catalytic behavior of the virus-bound enzymes. The observation of an extended plateau current in the $E >> E°$ region demonstrates that, due to its large excess, consumption of glucose by the enzymatic reaction is negligible and the glucose concentration sensed by the enzyme is the bulk concentration $C_G^\circ$, i.e., $[G] = C_G^\circ$ in Equation (2). Hence, as a benefit of the experimental configuration explored here, kinetic information can be obtained without interference from substrate or cosubstrate mass transport limitations.

Importantly, we observed that the intensity of the plateau current $i_{cat,\,pl}$ is also a function of the virus coverage, $\gamma_{fd}$. This is evidenced in Figure 2C where catalytic voltammograms acquired at surfaces of various virus coverages are reproduced, but also in **Figure 3**A, where a large set of $i_{cat,\,pl}$ versus $\gamma_{fd}$ data is plotted. Demonstrating that it is the GOx molecules specifically bound to the virus that are electrochemically interrogated and not nonspecifically adsorbed enzymes.

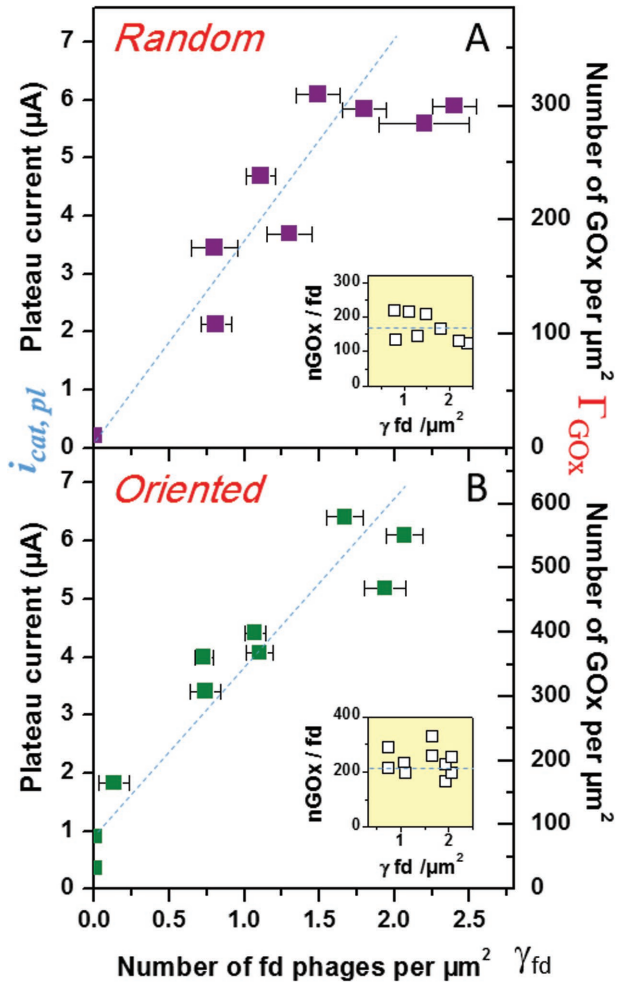


**Figure 3.** Intensity of the catalytic plateau current, $i_{cat,\,pl}$, recorded at electrodes bearing either A) random or B) oriented nanoarrays of GOx-decorated fd bacteriophages as a function of fd surface coverage, $\gamma_{fd}$. The right *Y*-axis is the overall electrode GOx coverage, $\Gamma_{GOx}$ in molecules $\mu m^{-2}$, calculated from each $i_{cat,\,pl}$ value as described in the text. The insets show the number of GOx molecules borne by fd-viruses, $n_{GOx}$, as given by the $\Gamma_{GOx}/\gamma_{fd}$ ratio calculated for each data point.

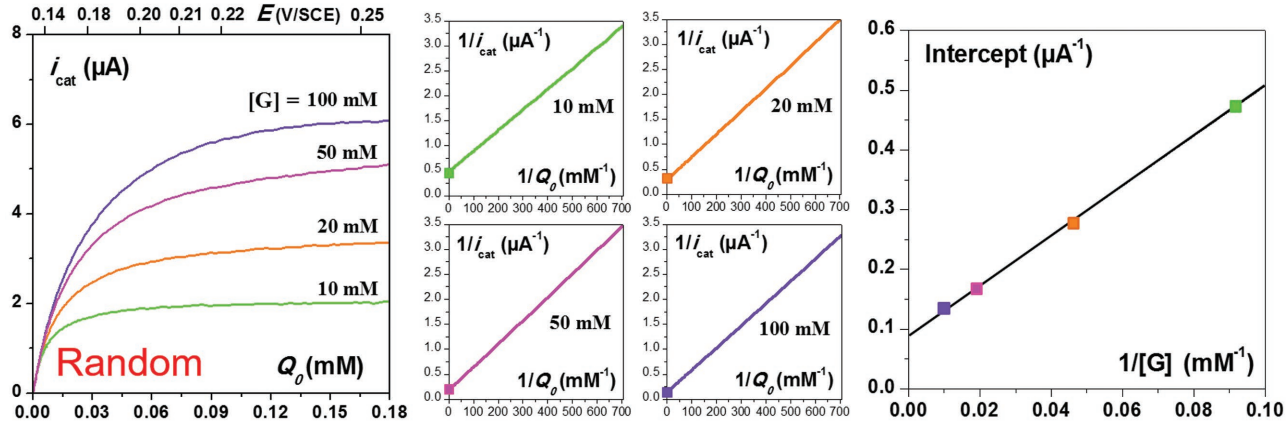


**Figure 4.** Kinetic characterization of random nanoarrays of GOx-decorated fd bacteriophages. (Left) Variation of the catalytic current $i_{cat}$ as a function of $Q_0$, the concentration of cosubstrate (ferroceniumdimethanol) at the electrode surface calculated from the electrode potential $E$ displayed as the upper $X$-axis of the graph. Each curve corresponds to a different glucose concentration as indicated. (Center) Lineweaver–Burk-like primary plots showing the reciprocal of the catalytic current ($1/i_{cat}$) as a function of $1/Q_0$, the square symbol marks the intercept of the plots. The glucose concentration is indicated on each plot. (Right) Secondary plot where the intercepts of the primary plots are reported as a function of the reciprocal of glucose concentration. Ferrocenedimethanol $0.25 \times 10^{-3}$ M in PB buffer pH 7.4. $T = 25$ °C. $\gamma_{fd} \approx 1.5$ particles μm$^{-2}$. $S \approx 0.466$ cm$^2$.

Indeed, in the absence of virus ($\gamma_{fd} = 0$) a weak and distorted $i_{cat}$ versus $E$ signal was obtained (Figure 2C, lower trace), pointing to negligibly trace amounts of GOx-conjugate on the surface.

The kinetic behavior of scaffolded GOx molecules can be quantitatively analyzed using the $i_{cat}$ versus $E$ purely catalytic signal as the electrode potential, $E$, corresponds to the cosubstrate concentration, $Q_0$. The exact value of $Q_0$ is calculated from Equation (3) and varies all along the potential scan, from $0 \times 10^{-3}$ M at the foot of the voltammogram up to $C^{\circ}_P$ ($0.25 \times 10^{-3}$ M) in the plateau region. As a result, the $i_{cat}$ versus $E$ voltammograms can be directly converted into $i_{cat}$ versus $Q_0$ kinetic curves reflecting the dependence of the enzymatic rate on the cosubstrate concentration. A series of such experimental curves, corresponding to various glucose concentrations, are plotted in **Figure 4** (left) and display the typical "saturating" behavior characteristic of enzyme kinetics.

Classical Lineweaver–Burk primary plots were then derived from these raw kinetic curves by plotting $1/i_{cat}$ as a function of $1/Q_0$. One can see from Figure 4 (center) that perfectly linear $1/i_{cat}$ variations are then obtained over an extremely wide range of $1/Q_0$ values, corresponding to actual cosubstrate concentration at the electrode in the $1 \times 10^{-6}$ to $0.25 \times 10^{-3}$ M range. The observed linearity evidences that the scaffolded GOx molecules obey Michaelis–Menten kinetics, confirming the starting assumption, see Equation (2) above. Hence, for the quantitative interpretation of the primary plots, one can justifiably make use of the following theoretical expression derived from Equation (2)

$$\frac{1}{i_{cat}} = \frac{K_M^{Fc}}{2Fn_E k_{cat}}\left(\frac{1}{Q_0}\right) + \frac{1}{2Fn_E k_{cat}}\left(1 + \frac{K_M^G}{C^{\circ}_G}\right) \quad (4)$$

As predicted by this latter equation, the primary plots corresponding to the range of glucose concentrations explored form nicely parallel lines (see Figure 4, center) and from their common slope a value for the first global parameter was obtained, $K_M^{Fc}/(2Fn_E k_{cat})$. The intercept of the primary plots as a function of the reciprocal of glucose concentration yielded the secondary plot shown in Figure 4 (right). The slope and the intercept of this plot provided the value for the second global parameter, $K_M^G/(2Fn_E k_{cat})$, and the $1/(2Fn_E k_{cat})$ ratio, respectively. These values were then used to derive two individual Michaelis constants that characterize glucose oxidase enzyme kinetics: $K_M^G = (50 \pm 20) \times 10^{-3}$ M, $K_M^{Fc} = (50 \pm 7) \times 10^{-6}$ M (averaged from three repeats).

The value of the rate constant $k_{cat}$ can be derived from the experimental value of the $1/(2Fn_E k_{cat})$ ratio provided the value of $n_E$ is determined independently from any kinetic measurement. To perform such a delicate determination, a highly trustful protocol was implemented (fully detailed in the Supporting Information) to mildly denature GOx to release FAD, which was then assayed by fluorescence. Experimentally, $n_E$ values in the 0.03–0.08 pmol range were measured for the relatively densely populated ($\gamma_{fd} \approx 1.5$–$2.4$ particles μm$^{-2}$) nanoarrays purposefully used for our kinetic studies.

From the values of $n_E$ and of the $1/(2Fn_E k_{cat})$ ratio determined for the same electrodes, an average value for $k_{cat} = 1000 \pm 300$ s$^{-1}$ was ultimately derived. Indeed by proceeding in this way we implicitly assumed that all of the GOx molecules present on the surface were catalytically active. This seems reasonable considering that the immunoassembly process is known to preserve GOx's activity.[16]

### 2.3. Estimating the Enzyme Coverage on fd Random Arrays

The number of GOx molecules borne by the randomly arrayed fd particles ($n_{GOx}$) can be estimated if one knows, for each surface examined, both the virus coverage, $\gamma_{fd}$, and the number of GOx molecules per unit surface area, i.e., the GOx coverage, $\Gamma_{GOx}$. Since there are two FAD moieties per GOx molecule,[22] $\Gamma_{GOx}$ is related to $n_E$ by $\Gamma_{GOx} = n_E N/(2S)$, where $N$ is the Avogadro number and $S$ is the area of the gold surface.

Having obtained all of the kinetic constants ($k_{cat}$, $K^{Fc}{}_M$, $K^G{}_M$), the value of $n_E$ can directly be determined simply from the intensity of the catalytic plateau current $i_{cat,\ pl}$ recorded at each of the surfaces interrogated, by applying Equation (2) with $Q_0 = C^\circ{}_p$. This allows us to rescale the $i_{cat,\ pl}$ versus $\gamma_{fd}$ plot in Figure 3A into a $\Gamma_{GOx}$ versus $\gamma_{fd}$ plot. One can see from this figure that $\Gamma_{GOx}$ increases approximately linearly with $\gamma_{fd}$ within the region where $\gamma_{fd}$ = 0–1.8 particles μm$^{-2}$, but begins to plateau when $\gamma_{fd}$ is further increased. These results show that, when $\gamma_{fd} < 2$ particles μm$^{-2}$, virus particles are decorated by a constant number of GOx molecules independently from the virus coverage on the electrode. This number is given by the slope of the linear fit to the $\Gamma_{GOx}$ versus $\gamma_{fd}$ data set, which yields a value of $n_{GOx}$ = 175 GOx molecules per fd particle. At higher $\gamma_{fd}$ coverages, the number of GOx molecules decorating the virus can be derived for each of the data points by calculating the $\Gamma_{GOx}/\gamma_{fd}$ ratio. It can be seen in the inset of Figure 3A, that in this region viruses are decorated by only ≈130 GOx molecules. This lower $n_{GOx}$ value may be due to the fact that, with high virus coverages, a significant fraction of the adsorbed phage particles are intertwined and display limited accessibility for the primary antibody and the GOx-antibody conjugate.

It is interesting to compare the experimentally obtained GOx coverage to the maximum number that can decorate the surface of fd particles, which can be estimated based on the following geometric considerations. The accessible outer surface area of fd is of 18 700 nm$^2$;[13] in the adsorbed state it is assumed about half of its surface is actually masked by the electrode. Taking 100 nm$^2$ as the footprint of an IgG, it is thus estimated that the adsorbed virus can accommodate ≈100 primary anti-fd capsid antibodies.[19] Assuming that each primary antibody can be recognized by 2–3 IgG-GOx molecules, a reasonable assumption due to their polyclonality, it can be estimated that 200–300 GOx molecules at most can be immobilized on each viral particle. Comparing this figure to the experimental GOx coverage on fd a maximum packing coverage of 65%–90% is evident. Notably, such a high yield decoration of individual fd particles by active enzyme molecules has never been reported to date. Recently, a record of ≈90 copies of the relatively large green fluorescent protein (27 kDa) has been assembled on M13 using an original sortase-mediated virus modification method.[23] Our results demonstrate that a significantly higher number of the much larger GOx enzyme molecule (150 kDa) can be displayed on fd by immunodecoration. This finding is in agreement with other studies which have shown that affinity-based methods allow high yield decoration of plant viruses by enzyme molecules.[5d,9j,24]

### 2.4. Assembly of an Oriented Array of GOx Immunodecorated fd

One of the interests of using viruses as nanocarriers, especially linear viruses, is that, in spite of their nanometric size, they can be manipulated using a variety of techniques to form ordered patterns.[10] Indeed, it has been reported that bacteriophage M13, differing from fd by only a single amino-acid change in the major coat protein P8, can be patterned into nanoarrays of oriented viruses on various surfaces, such as graphene oxide,[25] $SiO_2$,[26] or polymer surfaces,[27] via a simple molecular combing technique.[28] Molecular combing relies on the shear forces generated by a recessing meniscus to align high aspect ratio macromolecules at interfaces.[28] This technique was used herein to align fd viruses on bare TS-gold by depositing a solution of fd in PB pH 7.4 for 5 min, followed by molecular combing at ≈45° angle, causing the drop to tip over (see **Figure 5**A). A gentle flux of nitrogen was simultaneously flowed over the tilted sample, in the direction of the recessing water droplet, in order to complete drying of the surface. Tapping mode AFM imaging in air of the surface confirmed orientated and well individualized fd nanoarrays on the bare gold surface (Figure S4, Supporting Information). The particles were observed to be oriented along the drying direction, i.e., perpendicularly to the recessing water drop meniscus. Interestingly, we observed that orientation of fd particles was only possible on bare gold surfaces and not on cysteamine modified surfaces, likely due to strong electrostatic binding of fd to cysteamine inhibiting virus orientation after adsorption.

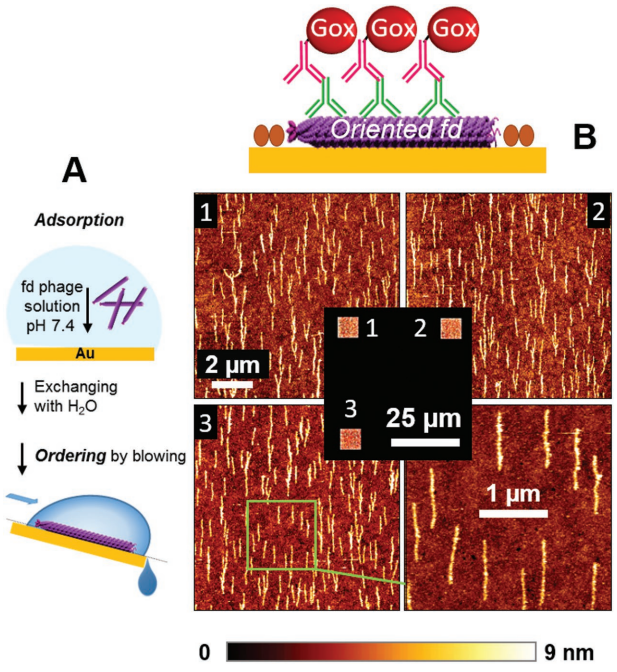


**Figure 5.** A) Schematic of the molecular combing technique used to produce nanoarrays of highly oriented fd particles on bare gold. B) In situ tapping mode AFM images of a surface showing the oriented viral particles after immunodecoration by GOx, as schematically represented by the cartoon above the images. The black frame in the center shows the locations where the images were acquired, illustrating the high degree of conservation of the viral orientation along the surface. $[fd]_{ads}$ = 1.9 μg mL$^{-1}$. $\gamma_{fd}$ ≈ 1.9 particles μm$^{-2}$.

Following orientation, the surface was then rehydrated with buffer and blocked by BSA adsorption. Immunodecoration of the virus particles by GOx was carried out as described above for the random particle nanoarrays. In situ AFM imaging was employed to monitor each assembly step and, importantly, showed that minimal desorption of virus

  

particles from the surface occurred during each step. This is likely due to reinforced attachment of adsorbed fd virus particles to gold surfaces as a benefit from the drying process during molecular combing.[18a]

The final result was a dense nanoarray of oriented GOx-fd with minimal overlap, Figure 5B, where the directional order of the nanoarrays was found to be preserved over domains many hundreds of micrometers across. The surface concentration of virus, $\gamma_{fd}$, was varied from 0.1 to 2 particles $\mu m^{-2}$ by adjusting the concentration of the fd solution used for adsorption (see Figure S1, Supporting Information).

### 2.5. Probing the Catalytic Activity of Oriented GOx-fd Nanoarrays and Determination of the GOx Coverage on Oriented Viruses

The kinetic behavior of oriented GOx-fd nanoarrays was studied by CV as described above for the random nanoarrays. High quality kinetic data were obtained from careful analysis of purely catalytic CVs (see **Figure 6**), yielding the following values for the enzyme kinetic constants; $K_M^G = (30 \pm 6) \times 10^{-3}$ M, $K_M^{Fc} = (35 \pm 8) \times 10^{-6}$ M, and $k_{cat} = 500 \pm 150\ s^{-1}$ (average values out of three replicates).

Using this set of kinetic constants the GOx coverage, $\Gamma_{GOx}$, for each surface bearing oriented GOx-fd nanoarrays was calculated. The obtained $\Gamma_{GOx}$ versus $\gamma_{fd}$ dataset is plotted in Figure 3B. One can see in this figure that $\Gamma_{GOx}$ increases linearly with $\gamma_{fd}$ over the whole range of virus coverage explored (0–2.1 particles $\mu m^{-2}$), with no sign of leveling off at high $\gamma_{fd}$ values. This behavior contrasts with what was observed for random GOx-fd arrays and illustrates a benefit of orientating the phage particles:particle intertwinement is avoided and the whole virus capsid remains accessible for the antibodies to decorate even when forming relatively dense arrays.

From the slope of the $\Gamma_{GOx}$ versus $\gamma_{fd}$ plot (dotted line in Figure 3B), an average number of $n_{GOx} = 220$ GOx molecules per oriented virus particle was determined. This amounts to a 75%–100% coverage of the fd surface and is noticeably higher than that for random GOx-fd arrays, confirming that oriented viruses are more prone to immunodecoration than randomly adsorbed viruses.

The origin of the line of best fit, shown in Figure 3B, suggests that about 100 GOx molecules $\mu m^{-2}$ were nonspecifically adsorbed on these surfaces and is likely due to the limited ability of BSA to block nonspecific adsorption on bare gold.[29] However, these molecules were found to have a negligible effect on the kinetic analysis of the activity of oriented GOx-fd arrays, as these experiments were carried out on surfaces displaying high virus coverages (≈1.5–2 particles $\mu m^{-2}$) corresponding to over 500 GOx $\mu m^{-2}$.

### 2.6. Immunoassembly and Kinetic Characterization of "Reference" GOx Monolayers on TS-Gold and Cysteamined TS-Gold

In order to have "reference" systems, where GOx would be immobilized on a surface but not confined to a nanoscaffold, we assembled immunologically monolayers of GOx both on bare and cysteaminated TS-gold electrodes. Following a previously reported protocol,[17] a monolayer of rabbit IgG molecules was first adsorbed onto the electrodes and, after a BSA blocking step, the rabbit IgGs were recognized by the antirabbit GOx conjugate used throughout this study. The enzymatic activity of the resulting immunoassembled GOx monolayers was characterized by CV, and its FAD content assayed as described in the Supporting Information, yielding the values of rate constants reported in **Table 1**. In order to allow for comparison with published data, these rate constants were also measured in 0.1 M ionic strength PB, pH 8, the working medium used in early works,[16] and are reported in Table S1 (Supporting Information). The kinetic values obtained for the reference monolayers are consistent with values reported in literature and in agreement with those of the native enzyme in solution, hence, verifying the immunologically scaffolded GOx molecules were active.

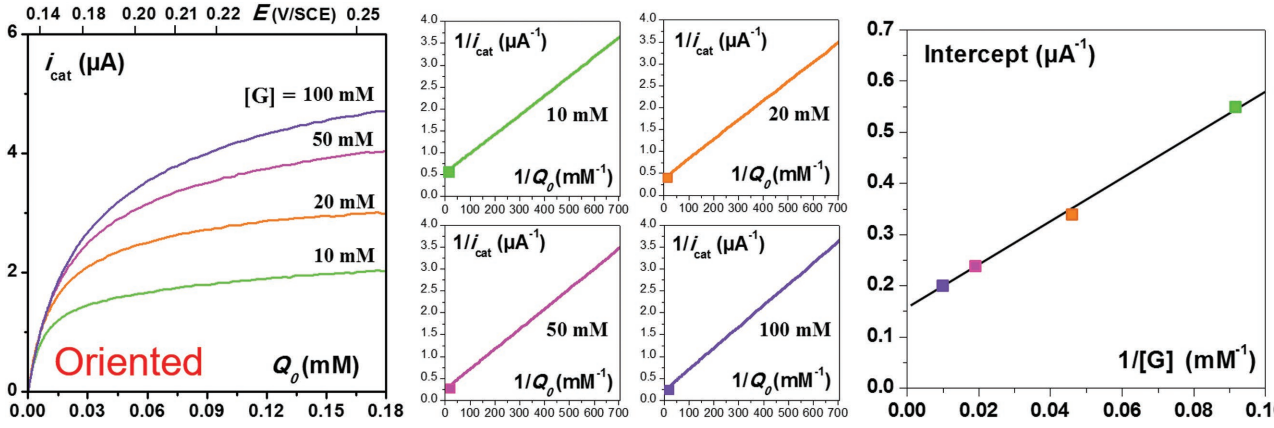


**Figure 6.** A) Schematic of the molecular combing technique used to produce nanoarrays of highly oriented fd particles on bare gold. B) In situ tapping mode AFM images of a surface showing the oriented viral particles after immunodecoration by GOx, as schematically represented by the cartoon above the images. The black frame in the center shows the locations where the images were acquired, illustrating the high degree of conservation of the viral orientation along the surface. $[fd]_{ads} = 1.9\ \mu g\ mL^{-1}$. $\gamma_{fd} \approx 1.9$ particles $\mu m^{-2}$.

  

**Table 1.** Kinetic constants for the enzymatic activity of random and oriented GOx-fdnanoarrays, and a monolayer of GOx, in $10 \times 10^{-3}$ M PB, pH 7.4. Mediator: Ferrocenedimethanol. The error margins represent standard deviation of (at least) triplicate experiments. $T = 25$ °C.

| Kinetic constants | GOx-fd nanoarrays | | GOx monolayer on bare gold | GOx monolayer on cysteaminated gold |
|---|---|---|---|---|
| | Random | Oriented | No fd | No fd |
| $K_M^G$ [$\times 10^{-3}$ M] | 50 ± 20 | 30 ± 6 | 35 ± 20 | 20 ± 10 |
| $K_M^{FC}$ [$\times 10^{-6}$ M] | 50 ± 7 | 35 ± 8 | 35 ± 10 | 35 ± 10 |
| $k_{cat}$ [$s^{-1}$] | 1000 ± 300 | 500 ± 150 | 450 ± 100 | 260 ± 80 |
| $k_{ox}$ [$M^{-1}$ $s^{-1}$] | $(2.1 \pm 0.6) \times 10^7$ | $(1.9 \pm 0.6) \times 10^7$ | $(1.2 \pm 0.3) \times 10^7$ | $(0.8 \pm 0.3) \times 10^7$ |
| $k_{red}$ [$M^{-1}$ $s^{-1}$] | $(2.9 \pm 0.8) \times 10^4$ | $(1.7 \pm 0.5) \times 10^4$ | $(1.4 \pm 0.4) \times 10^4$ | $(1.3 \pm 0.4) \times 10^4$ |

### 2.7. Catalytic Activities of GOx-fd Nanoarrays: Searching for Scaffolding and Orientational Kinetic Effects

Kinetic constants characterizing the activity of GOx, either immunoassembled as monolayers, or confined onto random/oriented fd nanoarrays, are collected in Table 1. For the ease of discussion, and for comparison with earlier works on GOx kinetics, the value of the rate constants $k_{ox}$ and $k_{red}$ are also given. These values were calculated from the set of kinetic constants, $K_M{}^G$, $K_M{}^{Fc}$, $k_{cat}$ experimentally determined herein, using the relations $k_{ox} = k_{cat}/K_M^{Fc}$ and $k_{red} = k_{cat}/K_M^G$.

$k_{ox}$ was introduced in the kinetic scheme shown above and characterizes the rate of oxidation of the enzyme flavin by $Fc^+$. $k_{red}$ is the so-called specificity constant of the enzyme, measuring the efficiency of GOx to convert glucose into gluconolactone.

Table 1 shows all kinetic constant values acquired for the random GOx-fd nanoarrays are higher than for the reference GOx monolayer assembled on cysteaminated gold. In particular, the catalytic constant $k_{cat}$, which reflects the enzyme's maximum rate, is markedly higher and evidences an enhancement in the intrinsic catalytic activity of GOx when confined to the capsid of randomly adsorbed phage particles. The fact that both of the $K_M$ values are also higher for the random GOx-fd nanoarray system is consistent with an increased $k_{cat}$ value since, by definition $K_M^{Fc} = k_{cat}/k_{ox}$ and $K_M^G = (k_{cat} + k_{-1})/k_1$. Note that $K_M$'s are kinetic and not affinity constants, their variation cannot be straightforwardly interpreted as a modulation of the enzyme affinity for its substrate or cosubstrate, as is often done in literature.

Interestingly, it can also be seen from Table 1 that the $K_M^G/K_M^{Fc} = k_{ox}/k_{red}$ ratio is largely preserved when passing from the GOx monolayer to the random GOx-fd nanoarray, indicating that $k_{ox}$ and $k_{red}$ were similarly affected by confinement of the enzyme on the virus. This is confirmed by examining the values given in Table 1 for these rate constants where one can see that both increased to a similar extend.

For the case of oriented GOx-fd nanoarrays, values for all the kinetic constants are, within experimental uncertainties, identical to those for the GOx monolayer on bare gold, indicating that the activity of GOx is fully preserved upon confinement. However, no catalytic enhancement of GOx activity was observed, hence, mere confinement of GOx to the virus particle is not sufficient to increase the enzyme activity. The results obtained herein show that randomly arranged nanocarriers favor enhancement rather than an oriented fd, hence arrangement is key to enhancing catalysis. There is no clear-cut explanation for this unprecedented result. Importantly, one cannot attribute the enhancement of GOx activity on randomly oriented viruses to the cysteamine anchoring layer, as the catalytic constants for the reference GOx monolayer assembled on bare gold and on cysteaminated gold are comparable within error (see Table 1) and, if anything, displays a somewhat lower $k_{cat}$ value.

We note that enhanced activity of GOx has previously been reported for substantially different "disordered" scaffolded systems, characterized in solution, where the enzyme was decorating gold nanoparticles.[30] However, to the best of our knowledge, this work is the first report of catalytic enhancement for an enzyme attached to a filamentous virus nanocarrier.

## 3. Conclusion

The enzymatic activity of random and oriented GOx-fd nanoarrays on gold surfaces was carefully studied. Immunodecoration allowed fully active enzyme molecules to be specifically assembled onto surface-immobilized viruses. Higher enzyme coverage of virus particles was observed for oriented fd nanoarrays, 220 GOx per fd corresponding to full saturation, compared to randomly oriented viruses, 175 GOx molecules per fd corresponding to 65% coverage.

The kinetic analysis carried out on random and oriented GOx-fd nanoarrays showed that neither the confinement of the enzymes onto the virus, nor the orientation of the virus particles affected the mechanism of GOx-catalyzed glucose oxidation, which closely followed Michaelis–Menten kinetics. However, a clear kinetic effect was observed in the case of the random system which displayed enhanced catalysis compared to the monolayer system. This enhancement was rooted to a twofold increase in the catalytic rate constant $k_{cat}$ and a more modest increase in the enzyme's $K_M$'s. These results provide clear evidence of catalytic enhancement due to scaffolding of a redox enzyme on a filamentous viral particle. Yet, most surprisingly, kinetic analysis of the oriented system did not show any sign of such an enhancement, providing the first ever evidence that orientation of virus particles can also modulate the activity of virus-scaffolded enzymes.

The original experimental platform implemented here, where enzyme-decorated phages are directly assembled on a flat electrode surface, allowing for kinetic interrogation and structural characterization, is a promising and convenient new approach to studying the scaffolding effects on enzymatic

  

activity, opening up new perspectives for further broadening the scope of phage-based electrochemical applications.

## 4. Experimental Section

*Biological Material: Virus Particles*: Viruses were grown using an ER2738 strain as *E. coli* host bacteria and purified following standard biological protocols.[31] Yields of ≈10 g of bacteriophages per liter of infected bacteria culture were typically obtained. For this work, virus suspensions (≈4 mg $mL^{-1}$) were extensively dialyzed against $10 \times 10^{-3}$ M sodium phosphate buffer pH 7.4 and stored at 4 °C until further use.

*Primary and Secondary Antibodies*: Primary anti-fd polyclonal antibody (IgG) produced in rabbit was obtained from Sigma-Aldrich. Secondary GOx (from *Aspergillus Niger*)-conjugated antirabbit polyclonal antibody produced in goat was acquired from Covalab (France). The secondary unconjugated polyclonal goat antirabbit IgG (for negative controls), the sacrificial rabbit IgG (for testing GOx monolayers in reference systems), and the BSA (IgG-free grade) blocking agent were from Jackson ImmunoResearch Laboratories.

*Chemicals and Solutions*: All chemicals were analytical grade Sigma-Aldrich products and used as received. All solutions were prepared with double-deionized water (18.2 MΩ cm resistivity, TKA Micro-Pure UV). A solution of $10 \times 10^{-3}$ M PB at pH 7.4 was used throughout and 0.1% sodium azide was added as a preservative to the antibody solutions if used for longer than a few hours. All solutions and systems were protected from light with aluminum foil during investigation and storage.

*Preparation of the Gold Surfaces*: Ultraflat gold surfaces were produced by TS of a 200 nm thick gold layer deposited on mica, as previously described.[32] An adhesive perforated Teflon mask was then glued to the gold surface, leaving a disk-shaped area of bare gold 0.76 cm in diameter.

*Preparation of Cysteaminated Gold Surfaces*: Gold surfaces were treated with $5 \times 10^{-3}$ M cysteamine, hydrochloride ($HS-(CH_2)_2-NH_3^+$, $Cl^-$), for 2 h under a water-saturated nitrogen atmosphere. The surface was then thoroughly rinsed by droplet replacement of cysteamine with water (twice) and then with PB pH 7.4 (twice). Drop replacement was cautiously carried out to avoid drying of the surface. Note, thiol-functionalized surfaces were kept under a water-saturated nitrogen atmosphere in all subsequent assembly steps to prevent oxidative desorption of the cysteamine layer from gold.

*Adsorption of Random fd Nanoarrays on Cysteaminated Gold*: A 70 µL solution of PB pH 7.4 containing fd viruses at 0.5 to 2 µg $mL^{-1}$ ($(0.25–1) \times 10^{11}$ phage particles $mL^{-1}$) was deposited onto the cysteaminated gold surface for 5 min, followed by two drop replacement rinsing steps with buffer for 20 min each for the desorption of any weakly bound material.

*Adsorption and Molecular Combing of fd on Bare Gold for Oriented Nanoarrays*: A 70 µL solution of PB pH 7.4 containing fd viruses at 0.1–2 µg $mL^{-1}$ was deposited onto a bare TS gold surface for 5 min, the surface was rinsed twice with buffer and once with water by drop replacement. The surface was then tilted at ≈45° to tip off the water drop, whilst simultaneously blowing a gentle flow of nitrogen over the surface for 10 s, completely drying the surface. The surface was then rehydrated by a drop of PB.

*Protective BSA Backfilling*: Virus bearing surfaces were backfilled with a protective BSA layer by adsorption from a 70 µL drop of 2 mg $mL^{-1}$ BSA in PB for: 1 h for random arrays on cysteamine, and 2 h for oriented arrays on bare gold, as BSA blocking of bare gold was not as good as on cysteaminated surfaces.

*Assembly of the Primary (Anti-fd) Antibody*: The surface was rinsed and left in contact for 45 min with a 5 µg $mL^{-1}$ (≈$1.5 \times 10^{13}$ molecules $mL^{-1}$) solution of the primary anti-fd rabbit antibodies.

*Assembly of the Secondary GOx-Conjugated Antibody*: Surfaces bearing random virus arrays were left overnight in contact with a 20 µg $mL^{-1}$ solution of the secondary antirabbit IgG-GOx conjugate. Surfaces bearing oriented virus arrays were first left in buffer overnight, in order to desorb any loosely adsorbed primary antibody molecules, before being exposed to a 10 µg $mL^{-1}$ solution of the IgG-GOx conjugate for 4 h. This latter protocol aimed at minimizing nonspecific binding of GOx-conjugated antibodies to the surface, which was found to be harder to prevent on surfaces that were not treated with cysteamine—in order to allow for fd orientation—likely due to less effective BSA blocking (see above).

Experimental conditions (time, concentration) were adapted for the assembly of the primary and secondary antibody layers onto the fd particles in order to bring the antigen-antibody recognition reactions to completion based on previous studies on similar immunoconstruction,[16] and viral particle decoration by redox antibodies.[17] Surfaces were stored at room temperature, in PB containing 0.1% sodium azide. The surfaces bearing a cysteamine layer were placed in a water-saturated nitrogen atmosphere.

*AFM Imaging*: Tapping mode AFM images were acquired with a Nanowizard II microscope (JPK, Germany). In situ (i.e., in buffer) imaging was carried out with V-shaped contact mode probes (MLCT-AUMN or MSNL-10, Brucker, spring constant 0.1 N $m^{-1}$, tip curvature 20 nm). For in air imaging rectangular contact mode probes (PPP-CONTR-10, Nanosensors, spring constant 0.2 N $m^{-1}$, tip curvature 10 nm) were used. No correction other than first degree flattening was applied to the images.

*Electrochemical Analysis*: The surface was mounted at the bottom of a jacketed glass cell, equipped with an O'ring, designed and fabricated in-house. CVs were recorded with a CHI630C electrochemical workstation, in a three electrode configuration with a platinum wire counter and a micro-Ag/AgCl reference electrode (3 M KCl, World Precision Instruments), at 25 °C using a circulating water bath. All potentials in this work are reported versus the KCl saturated calomel reference electrode (SCE) (+47 mV versus Ag/AgCl, KCl 3 M). Measurements were carried out in deoxygenated solutions that were maintained under an $N_2$ atmosphere inside the cell. Note, the stock solutions of glucose were allowed to mutarotate overnight, and deoxygenated before use.

*Fluorescence Assay of Enzyme-Bound FAD from GOx-fd Nanoarrays*: The fluorescence assay is fully detailed in the Supporting Information. Briefly, GOx-scaffolded fd surfaces were treated with PB pH 2.55 for 24 h in order to denature the enzymes and promote release of FAD into the solution, allowing the FAD concentration to be assayed using fluorescence.

## *Supporting Information*

*Supporting Information is available from the Wiley Online Library or from the author.*

  

## Acknowledgements

*This work received financial support by the French "Agence Nationale de la Recherche" (ANR) through "eVIRZYM" (DS0401 – ANR 2014-CE09-0009).*

[1] K. Jørgensen, A. V. Rasmussen, M. Morant, A. H. Nielsen, N. Bjarnholt, M. Zagrobelny, S. Bak, B. L. Møller, *Curr. Opin. Plant Biol.* **2005**, *8*, 280.

[2] a) J. Conrado, J. D. Varner, M. P. DeLise, *Curr. Opin. Biotechnol.* **2008**, *19*, 492; b) Y. Tu, F. Peng, A. Adawy, Y. Men, L. K. E. A. Abdelmohsen, *Chem. Rev.* **2016**, *116*, 2023; c) R. Chen, Q. Chen, H. Kim, K.-H. Siu, Q. Sun, S.-L. Tsai, W. Chen, *Curr. Opin. Biotechnol.* **2014**, *28*, 59.

[3] T. Michon, in *Enzyme Nanocarriers* (Eds: T. Michon, D. Cardinale), Pan Standford, Singapore **2016**, Introduction.

[4] a) D. Cardinale, N. Carette, T. Michon, *Trends Biotechnol.* **2012**, *30*, 369; b) F. Li, Q. Wang, *Small* **2014**, *10*, 230.

[5] a) J. Fu, L. Liu, Y. Liu, N. W. Woodbury, H. Yan, *J. Am. Chem. Soc.* **2012**, *134*, 5516; b) T. A. Ngo, E. Nakata, M. Saimura, T. Morii, *J. Am. Chem. Soc.* **2016**, *138*, 3012; c) D. P. Patterson, B. Schwarz, R. S. Waters, T. Gedeon, T. Douglas, *ACS Chem. Biol.* **2014**, *9*, 359; d) C. Koch, K. Wabbel, F. J. Eber, P. Krolla-Sidenstein, C. Azucena, H. Gliemann, S. Eiben, F. Geiger, C. Wege, *Front. Plant Sci.* **2015**, *6*, 1137; e) J. Besong-Ndika, M. Wahlsten, D. Cardinale, J. Pille, J. Walter, T. Michon, K. Mäkinen, *Front. Plant Sci.* **2016**, *7*, 89.

[6] a) O. Idan, H. Hess, *Curr. Opin. Biotechnol.* **2013**, *24*, 606; b) J.-L. Lin, L. Palomec, I. Wheeldon, *ACS Catal.* **2013**, *4*, 505.

[7] a) B. J. Johnson, W. R. Algar, A. P. Malanoski, M. G. Ancona, I. L. Medintz, *Nano Today* **2014**, *9*, 102; b) O. Stueker, V. A. Ortega, G. G. Goss, M. Stepanova, *Small* **2014**, *10*, 2006.

[8] S. Ding, A. A. Cargill, I. L. Medintz, J. C. Claussen, *Curr. Opin. Biotechnol.* **2015**, *34*, 242.

[9] a) W. F. Rurup, M. S. T. Koay, J. J. L. M. Cornelissen, in *Enzyme Nanocarriers* (Eds: T. Michon, D. Cardinale), Pan Standford, Singapore **2016**, Ch. 3; b) M. Comellas-Aragonès, H. Engelkamp, V. I. Claessen, N. A. J. M. Sommerdijk, A. E. Rowan, P. C. M. Christianen, J. C. Maan, B. J. M. Verdiun, J. J. L M. Cornelissen, R. J. M. Nolte, *Nat. Nanotechnol.* **2007**, *2*, 635; c) N. Carette, H. Engelkamp, E. Akpa, S. J. Pierre, N. R. Cameron, P. C. M. Christianen, J. C. Maan, J. C. Thies, R. Weberskirch, A. E. Rowan, R. J. M. Nolte, T. Michon, J. C. M. van Hest, *Nat. Nanotechnol.* **2007**, *2*, 226; d) J. D. Fiedler, S. D. Brown, J. L. Lau, M. G. Finn, *Angew. Chem., Int. Ed.* **2010**, *49*, 9648; e) I. J. Minten, V. I. Claessen, K. Blank, A. E. Rowan, R. J. M. Nolte, J. J. L. M. Cornelissen, *Chem. Sci.* **2011**, *2*, 358; f) A. A. A. Aljabali, E. Barclay, N. F. Steinmetz, G. P. Lomonossoff, D. J. Evans, *Nanoscale* **2012**, *4*, 5640; g) D. P. Patterson, P. E. Prevelige, T. Douglas, *ACS Nano* **2012**, *6*, 5000; h) J. E. Glasgow, S. L. Capehart, M. B. Francis, D. Tullman-Ercek, *ACS Nano* **2012**, *6*, 8658; i) D. P. Patterson, B. Schwarz, K. El-Boubbou, J. van der Oost, P. E. Prevelige, T. Douglas, *Soft Matter* **2012**, *8*, 10158; j) J. Pille, D. Cardinale, N. Carette, C. Di Primo, J. Besong-Ndika, J. Walter, H. Lecoq, B. van Eldijk, F. C. M. Smits, S. Schoffelen, J. C. M. van Hest, K. Mäkinen, T. Michon, *Biomacromolecules* **2013**, *14*, 4351; k) R. A. Blaik, E. Lan, Y. Huang, B. Dunn, *ACS Nano* **2016**, *10*, 324.

[10] a) A. Cerf, C. Thibault, E. Trévisol, C. Vieu, in *Enzyme Nanocarriers* (Eds: T. Michon, D. Cardinale), Pan Standford, Singapore **2016**, Ch. 7; b) R. A. Vega, D. Maspoch, K. Salaita, C. A. Mirkin, *Angew. Chem., Int. Ed.* **2005**, *44*, 6013; c) A. Horn, S. Hiltl, A. Fery, A. Böker, *Small* **2010**, *6*, 2122; d) Y.-H. Shin, S.-H. Yun, S.-H. Pyo, Y.-S. Lim, H.-J. Yoon, K.-H. Kim, S.-K. Moon, S. W. Lee, Y. G. Park, S.-I. Chang, K.-M. Kim, J.-H. Lim, *Angew. Chem., Int. Ed.* **2010**, *49*, 9689.

[11] C. N. Seeman, A. M. Belcher, *Proc. Natl. Acad. Sci. USA* **2002**, *9*, 6451.

[12] a) F. J. Arévalo, A. González-Techera, M. A. Zon, G. González-Sapienza, H. Fernández, *Biosens. Bioelectron.* **2012**, *32*, 231; b) Z. Hosseinidoust, A. L. J. Olsson, N. Tufenkji, *Colloids Surf., B* **2014**, *124*, 2; c) M. Janczuk, J. Niedziółka-Jönsson, K. Szot-Karpińska, *J. Electroanal. Chem.* **2016**, *779*, 207.

[13] K. Zimmermann, H. Hagedorn, C. C. Heucks, M. Hinrichsen, H. Ludwig, *J. Biol. Chem.* **1986**, *261*, 1653.

[14] a) Q. H. Gibson, B. E. P. Swoboda, V. Massey, *J. Biol. Chem.* **1964**, *239*, 3927; b) M. K. Weibel, H. J. Brights, *J. Biol. Chem.* **1971**, *246*, 2734; c) O. Courjean, N. Mano, *J. Biotechnol.* **2011**, *151*, 122.

[15] C. Bourdillon, C. Demaille, J. Moiroux, J. M. Savéant, *J. Am. Chem. Soc.* **1993**, *115*, 2.

[16] C. Bourdillon, C. Demaille, J. Gueris, J. Moiroux, J. M. Savéant, *J. Am. Chem. Soc.* **1993**, *115*, 12264.

[17] L. Nault, C. Taofifenua, A. Anne, A. Chovin, C. Demaille, J. Besong-Ndika, D. Cardinale, N. Carette, T. Michon, J. Walter, *ACS Nano* **2015**, *9*, 4911.

[18] a) K. S. Zerda, C. P. Gerba, K. C. Hou, S. M. Goyal, *Appl. Environ. Microbiol.* **1985**, *49*, 91; b) Y. L. Lyubchenko, P. I. Oden, D. Lampner, S. M. Lindsay, K. A. Dunker, *Nucleic Acids Res.* **1993**, *21*, 1117; c) P. J. Yoo, K. T. Nam, A. Jifa, S.-K. Lee, J. Park, A. M. Belcher, P. T. Hammond, *Nat. Mater.* **2006**, *5*, 234.

[19] L. F. Pease, J. T. Elliot, D.-H. Tsai, M. R. Zachariah, M. J. Tarlov, *Biotechnol. Bioeng.* **2008**, *101*, 1214.

[20] Y. G. Kuznetsov, A. McPherson, *Microbiol. Mol. Biol. Rev.* **2011**, *75*, 268.

[21] J. Abbou, C. Demaille, M. Druet, J. Moiroux, *Anal. Chem.* **2002**, *74*, 6355.

[22] B. E. P. Swoboda, V. Massey, *J. Biol. Chem.* **1965**, *240*, 2209.

[23] G. T. Hess, J. J. Cragnolini, M. W. Popp, M. A. Allen, S. K. Dougan, E. Spooner, H. L. Ploegh, A. M. Belcher, C. P. Guimaraes, *Bioconjugate Chem.* **2012**, *23*, 1478.

[24] M. Bäcker, C. Koch, S. Eiben, F. Geiger, F. Eber, H. Gliemannd, A. Poghossiana, C. Wege, M. J. Schöning, *Sens. Actuators, B* **2017**, *238*, 716.

[25] Y. M. Lee, B. Jung, Y. H. Kim, A. R. Park, S. Han, W.-S. Choe, P. J. Yoo, *Adv. Mater.* **2014**, *26*, 3899.

[26] a) D.-Y. Jeon, K. H. Hwang, S.-J. Park, Y.-J. Kim, M.-K. Joo, S.-E. Ahn, G.-T. Kim, C.-H. Nam, *J. Appl. Phys.* **2011**, *109*, 064701; b) P. Moghimian, V. Srot, D. Rothenstein, S. J. Facey, L. Harnau, B. Hauer, J. Bill, P. A. van Aken, *Langmuir* **2014**, *30*, 11428.

[27] T. Sawada, T. Serizawa, *J. Mater. Chem. B* **2013**, *1*, 149.

[28] A. Bensimon, A. Simon, A. Chiffaudel, V. Croquette, F. Heslot, D. Bensimon, *Science* **1994**, *265*, 2096.

[29] K. Reimhult, K. Petersson, A. Krozer, *Langmuir* **2008**, *24*, 8695.

[30] a) L. Cao, J. Ye, L. Tong, B. Tang, *Chem. Eur. J.* **2008**, *14*, 9633; b) J. T. Holland, C. Lau, S. Brozik, P. Atanassov, S. Banta, *J. Am. Chem. Soc.* **2011**, *133*, 19262; c) H. He, X. Xu, H. Wu, Y. Zhai, Y. Jin, *Anal. Chem.* **2013**, *85*, 4546.

[31] J. Sambrook, E. F. Fritsch, T. Maniatis, *Molecular Cloning: A Laboratory Manual*, 2nd ed., Cold Spring Harbor, New York **1989**.

[32] K. Huang, A. Anne, M. A. Bahri, C. Demaille, *ACS Nano* **2013**, *7*, 4151.

Received: September 21, 2016
Revised: November 18, 2016
Published online: January 18, 2017

  